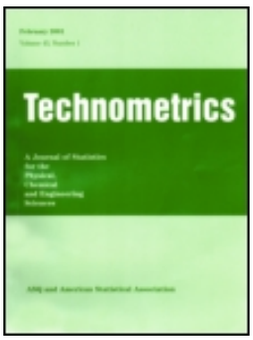

Technometrics

ISSN: 0040-1706 (Print) 1537-2723 (Online) Journal homepage: http://www.tandfonline.com/loi/utch20

Corrigendum

Yu Ding

To cite this article: Yu Ding (2017): Corrigendum, Technometrics, DOI: 10.1080/00401706.2017.1399710

To link to this article: http://dx.doi.org/10.1080/00401706.2017.1399710

TECHNOMETRICS
2017, VOL. 0, NO. 0, 1
https://doi.org/10.1080/00401706.2017.1399710

Taylor & Francis
Taylor & Francis Group

Corrigendum

Yu Ding

Department of Industrial & Systems Engineering, Texas A & M University, College Station, TX

In the article "Quantifying Nanoparticle Mixing State to Account for Both Particle Location and Size Effects," by L. Dong et al., *Technometrics*, 59(3), pp. 391–403, doi: 10.1080/00401706.2016.1186563, the author order was incorrect.

The corrected author order is as follows:

First author: Ling Dong, Academy of Mathematics and Systems Science, Chinese Academy of Sciences, Beijing, China

Second author: Xiaodong Li, Academy of Mathematics and Systems Science, Chinese Academy of Sciences, Beijing, China

Third author: Yanjun Qian, Department of Industrial & Systems Engineering, Texas A & M University, College Station, TX

Fourth author: Dan Yu, Academy of Mathematics and Systems Science, Chinese Academy of Sciences, Beijing, China

Fifth author: Hui Zhang, National Center for Nanoscience and Technology, Beijing, China

Sixth author: Zhong Zhang, National Center for Nanoscience and Technology, Beijing, China

Seventh author: Yu Ding, Department of Industrial & Systems Engineering, Texas A & M University, College Station, TX

Technometrics

ISSN: 0040-1706 (Print) 1537-2723 (Online) Journal homepage: http://amstat.tandfonline.com/loi/utch20

Quantifying Nanoparticle Mixing State to Account for Both Location and Size Effects

Ling Dong, Xiaodong Li, Dan Yu, Hui Zhang, Zhong Zhang, Yanjun Qian & Yu Ding

To cite this article: Ling Dong, Xiaodong Li, Dan Yu, Hui Zhang, Zhong Zhang, Yanjun Qian & Yu Ding (2017) Quantifying Nanoparticle Mixing State to Account for Both Location and Size Effects, Technometrics, 59:3, 391-403, DOI: 10.1080/00401706.2016.1186563

To link to this article: http://dx.doi.org/10.1080/00401706.2016.1186563

Accepted author version posted online: 11 May 2016.
Published online: 13 Apr 2017.

TECHNOMETRICS
2017, VOL. 59, NO. 3, 391–403
http://dx.doi.org/10.1080/00401706.2016.1186563

Taylor & Francis
Taylor & Francis Group

Quantifying Nanoparticle Mixing State to Account for Both Location and Size Effects

Ling Dong[a], Xiaodong Li[a], Dan Yu[a], Hui Zhang[b], Zhong Zhang[b], Yanjun Qian[c], and Yu Ding[c]

[a]Academy of Mathematics and Systems Science, Chinese Academy of Sciences, Beijing, China; [b]National Center for Nanoscience and Technology, Beijing, China; [c]Department of Industrial & Systems Engineering, Texas A & M University, College Station, TX

ABSTRACT

Ripley's *K* function is commonly used to characterize the homogeneity of spatial point distribution. Not surprisingly, it becomes a favored tool in quantifying the nanoparticles mixing state in composite materials, a parameter that material scientists believe is of close relevance to certain properties of the nanoparticle-embedding material. Ripley's *K* function assumes that the spatial points are dimensionless. In reality, the nanoparticles, once mixed in a host material, form clusters or agglomerates of various sizes and shapes. Our analysis shows that using the original *K* function falls short of ranking or distinguishing the homogeneity of nanoparticle mixing. We therefore propose to revise the *K* function to account for both particle location and size effects. We apply the revised function to electron microscopy images of material samples and conduct analysis and comparison of nanoparticle mixing. The analysis shows that the revised function is a better index to quantify the mixing states.

ARTICLE HISTORY
Received May 2015
Revised March 2016

KEYWORDS
Dispersion and distribution; Nano images; Permutation test; Ripley's *K* function; Spatial point pattern

1. Introduction

Material scientists have discovered that certain properties of a composite, for instance, the strength, conductivity or transparency, can be remarkably enhanced by blending nanoparticles into the polymer host material (Chang et al. 2006). The resulting improvement in material properties is believed to depend on how uniformly the nanoparticles are mixed into the host material (Zhang et al. 2006; Zeng, Yu, and Lu 2008). The importance of material mixing applies not only to nanoparticle-embedded materials but also to almost all other material mixing involving a host and additive or reinforcing agents (Manas-Zloczower 1997; Hui et al. 2008). Material scientists tend to describe the quality of a mixing state using two phrases: "dispersion" and "distribution." As illustrated in Figure 1 of Manas-Zloczower (1997), *dispersion* refers to the ability to break down agglomerates into small pieces, while *distribution* refers to the ability to make the additive agents (nanoparticles in this application), large or small, to locate uniformly throughout the host material. We also refer to the two effects as size (dispersion) and location (distribution) effects in this article.

Manas-Zloczower (1997) and Hui et al. (2008) stated that the ideal mixing state is good dispersion and good distribution. To accomplish that goal, material scientists employ different equipment or mechanisms (Ray and Okamoto 2003; Zou, Wu, and Shen 2008) to break down large-sized nanoparticle agglomerates into small pieces and try to make the small nanoparticle pieces (ideally, individual particles) distribute uniformly throughout the host material. Quantification of nanoparticle mixing provides an objective assessment and can sometimes serve as a surrogate for material properties. Doing so becomes a prerequisite to ensuring good quality of nanocomposites in its manufacturing process.

The quantification process starts with taking image measurements of a nanocomposite sample by using an electron microscope. The two most popular electron microscopes are the transmission electron microscope (TEM) and scanning electron microscope (SEM). In this research, all images are taken by TEMs, but we believe the resulting method and the associated discussion apply to SEM images as well.

Figure 1 shows a TEM image of the nanocomposite sample studied by our nanoscience team. The dark areas indicate the presence of nanoparticles or nanoparticle agglomerates. The TEM images are then processed by an image processing tool, for instance, `ImageJ` (Ferreira and Rasband 2011) or more sophisticated methods recently developed (Park et al. 2012, 2013). The image processing tool produces the contours of the nanoparticles and nanoparticle agglomerates, which can be used to calculate a particle's or an agglomerate's size and its centroid location. The size and location information is the common input to the subsequent quantification analysis of the mixing state.

Ripley's *K* function (Ripley 1976) is widely used in spatial statistics to characterize the homogeneity of spatial point distribution. The *K* function is a function of a specified distance *r* and is decided in part by the number of point pairs whose distance is shorter than *r*; the definition of the *K* function will be presented in Section 2. When the *K* function is used to quantify nanoparticle mixing state, it takes as inputs the centroid locations of the particles or particle agglomerates. Then its function value is computed assuming that each centroid is a dimensionless point. As a result, the *K* function in effect neglects distinc-

CONTACT Yu Ding *yuding@tamu.edu*
Color versions of one or more of the figures in this article are available online at *www.tandfonline.com/r/TECH*.

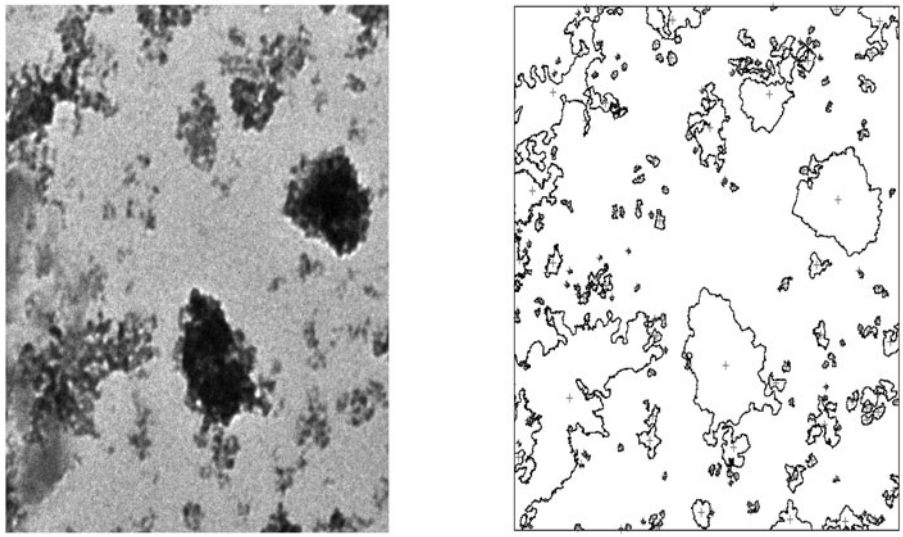

Figure 1. TEM image of a nanocomposite sample. From left to right: original TEM image; extracted agglomerate boundaries and centroids (indicated by the signs).

tion in the size of nanoparticle agglomerates and thus does not adequately account for the dispersion effect. The K function may work effectively, if the nanoparticles, despite not dimensionless, are of a uniform size and shape on a given material sample as well as across different samples, as under this circumstance, the size (or dispersion) effect is controlled for. It is indeed so in the study by Li et al. (2014), who show that when the particle size is homogenous and the shape of particles are spherical, Ripley's K function can be a reasonable metric to quantify the nanoparticle mixing state in a nanocomposite sample.

Despite the desire to break down nanoparticle agglomerates into small pieces of similar sizes, the agglomerates are difficult to avoid in reality, as evident in the TEM image in Figure 1. The resulting material inevitably contains particle agglomerates of various sizes and of irregular shapes. Obviously some physical processes disperse the particles better than other processes do, and it is indeed of great interest to the material scientists to find out which process, or process setting, does the job the best. But when the K function is applied to particle agglomerates of various sizes and shapes, it falls short of ranking or distinguishing nanoparticle mixing states; we will provide examples substantiating this claim later in Section 4.

We acknowledge that in addition to the K function, there exists other spatial homogeneity characterizing functions (Baddeley 2008). We believe that they make a similar dimensionless point assumption. Another school of thought in quantifying spatial homogeneity is to use the count-based approach, for instance, Zhou et al. (2014). But using the count-based approaches does not take the particle's size effect into account, either.

There are indeed revisions to the K function. One stream of work is to extend the K function to work for an underlying process of which the null hypothesis is not a homogenous spatial point process (Lotwick and Silverman 1982; Diggle and Chetwynd 1991; Diggle, Tawn, and Moyeed 1998; Baddeley, Møller, and Waagepetersen 2000), and for this reason, an adjustment must be made to the null hypothesis model. In our study, this extension is not relevant, as our null hypothesis still assumes a homogenous process. One study relevant to our undertaking is found in the application of forestry science (Penttinen, Stoyan, and Henttonen 1992; Stoyan and Penttinen 2000). The authors of the study noticed the mismatch between the dimensionless point assumption and some affiliating effect of tree stands (including size, economic value). They, hence, proposed to add a weight coefficient, related to the affiliating effect, in the calculation of the K function. We tried this approach in our study by including a particle size-based weight coefficient. It turns out that such a treatment does not address the problem; more evidence will be provided in Section 4.

In our research, to account for the size (dispersion) effect of particle agglomerates, we propose two actions to be conducted while using the K function. The first is to discretize the particle agglomerates into small enough, fine-scale particles and extract the centroid locations of the small particles for use in the K function. It turns out that this discretization action alone is still insufficient to solve the problem. An adjustment is needed on the normalizing parameter in the K function. The revised K function is referred to as the $\widetilde{K}$ function. To use the $\widetilde{K}$ function on samples, a nonparametric testing procedure, proposed by Diggle, Lange, and Beneš (1991); Diggle, Mateu, and Clough (2000) for the original K function, can still be used but we need to replace K with $\widetilde{K}$. We apply the $\widetilde{K}$ function to real TEM images of nanocomposite samples and show that the $\widetilde{K}$ function is a better index to quantify nanoparticle mixing states.

The remainder of this article is organized as follows. Section 2 introduces Ripley's K function and its weighted variant. Section 3 presents the $\widetilde{K}$ function, including both discretization and an adjustment to its normalizing parameter, and a nonparametric procedure for statistical testing. Section 4 shows the results of applying the $\widetilde{K}$ function to actual TEM images and presents the comparison analysis of nanoparticle mixing states over different samples. Section 5 concludes the article with additional discussions.

2. Ripley's *K* Function and Its Extension

Ripley's K function is defined as

$$K(r) = \frac{E(\text{number of extra points within distance } r \text{ of a randomly chosen point})}{\lambda}, \quad (1)$$

where E is the expectation operator and λ is the intensity of the point process, that is, the number of points per unit area. $K(r)$ has a close form expression under many spatial point models. The most commonly used ideal model is the complete spatial randomness (CSR) or homogeneous spatial Poisson process; under this ideal model, $K(r) = \pi r^2$.

Given an image containing a spatial point process, $K(r)$ can be estimated as follows. First, the number of points or particles in the image is counted and denoted by N. The area of the image is denoted by A. The intensity λ can then be estimated by $\hat{\lambda} = \frac{N}{A}$. We want to stress here that this $\hat{\lambda}$ is a *local* normalizing parameter as the microscopic images capturing nanoscale characteristics are always localized in a bulk material.

Denote by $d_{s_1 s_2}$ the Euclidean distance between point s_1 and s_2, $s_1, s_2 \in \{1, \ldots, N\}$. For the TEM images, $d_{s_1 s_2}$ is computed using the centroid coordinates of particles or particle agglomerates s_1 and s_2, which are available to us after the image processing step. Moveover, denoted by $I(x)$ the indicator function, namely $I(x) = 1$ when x is deemed "true" or $I(x) = 0$ otherwise. Then, the expected point number can be estimated by the average number of points within a given radius r of an arbitrarily chosen point. As such, the estimate of Ripley's K function is

$$\widehat{K}(r) = \frac{1}{N\hat{\lambda}} \sum_{s_1=1}^{N} \sum_{s_2 \neq s_1} I(d_{s_1 s_2} < r). \quad (2)$$

A larger $\widehat{K}$, as compared with the K value under the CSR assumption, implies clustering. The larger the $\widehat{K}$ value, the severer the clustering.

The above expression may run into problems when the reference point is very close to the boundary of an image, and consequently, part of the circle of radius r with the reference point as the center may be outside the image area. One commonly used correction is Ripley's isotropic correction (Ripley 1991), which is to assign a value between 0 and 1 to the circles that have part of their circumference outside the image area. So the corrected Ripley K function reads

$$\widehat{K}(r) = \frac{1}{N\hat{\lambda}} \sum_{s_1=1}^{N} \sum_{s_2 \neq s_1} w_{s_1 s_2} I(d_{s_1 s_2} < r), \quad (3)$$

where $w_{s_1 s_2}$ is the circumference proportion within the image area of a circle of radius $d_{s_1 s_2}$ and with point s_1 as the center.

As we mentioned in Section 1, Penttinen, Stoyan, and Henttonen (1992) introduced a K_{mm} function after noticing that some properties associated with a point may change the quantification of homogeneity. The K_{mm} function is an extension of the K function by adding a weight to each point s_1 or s_2. Let us first rewrite the K function in the following way:

$$K(r) = \frac{E\left(\sum_{s_1=1}^{N} \sum_{s_2 \neq s_1} I(d_{s_1 s_2} < r)\right)}{N\lambda}. \quad (4)$$

The K_{mm} function is a weighed version of Equation (4), that is,

$$K_{mm}(r) = \frac{E\left(\sum_{s_1=1}^{N} \sum_{s_2 \neq s_1} \mu_{s_1} \mu_{s_2} I(d_{s_1 s_2} < r)\right)}{N\lambda\mu^2}, \quad (5)$$

where μ_{s_1} and μ_{s_2} are the weights associated with the s_1th and s_2th points, respectively, and μ is the mean of all weights. An estimator of $K_{mm}(r)$ with a proper edge correction is

$$\widehat{K}_{mm}(r) = \frac{\sum_{s_1=1}^{N} \sum_{s_2 \neq s_2} \mu_{s_1} \mu_{s_2} w_{s_1 s_2} I(d_{s_1 s_2} < r)}{N\hat{\lambda}\hat{\mu}^2}, \quad (6)$$

where $\hat{\mu}$ is the average of the weights. Obviously, when the weights of each point are the same, that is, $\mu_{s_1} = \mu_{s_2} = \mu$, the K_{mm} is the same as Ripley's K function. The value of K_{mm} under null hypothesis is obtained when both weights and locations are completely randomly assigned.

Figure 2 presents a number of simulated images with different agglomerate types. Comparing this figure and Figure 1 in Manas-Zloczower (1997), Figure 2(a) resembles the "good dispersion, good distribution" graph (bottom-right of Figure 1 in Manas-Zloczower (1997); same below), Figure 2(b) resembles the "bad dispersion, good distribution" graph (top-right), while Figure 2(c) resembles the "bad dispersion, bad distribution" graph (top-left). When applying the original K function to the three images, it returns exactly the same value as the centroids of the agglomerates are the same. As expected, the K function ignores the dispersion (size) aspect altogether. When applying the K_{mm} function for which we use the agglomerate size as the weights, it does distinguish Figure 2(a) from Figure 2(c), or Figure 2(b) from Figure 2(c), but it still cannot distinguish Figure 2(a) from Figure 2(b). In Section 4, we present a real data example, in which K_{mm} shows very little differentiating ability.

3. The Revised $\widetilde{K}$ Function

3.1 Discretization

In revising Ripley's K function to account for the size effect of nanoparticle agglomerates, the first line of thought is to discretize the agglomerates into much smaller disjoint blocks. Then each block is treated as a new particle with its own centroid. By this action, the existence of large agglomerates is translated into a large number of small blocks that are closely clustered together. Presumably, Ripley's K function, once applied to the small-sized blocks, can reflect the closeness among them created by agglomerates, and consequently, distinguish the particle mixing states with and without aggregation. When the block sizes are small enough, then the remaining size effect, albeit not perfectly dimensionless, would hopefully no longer be significant.

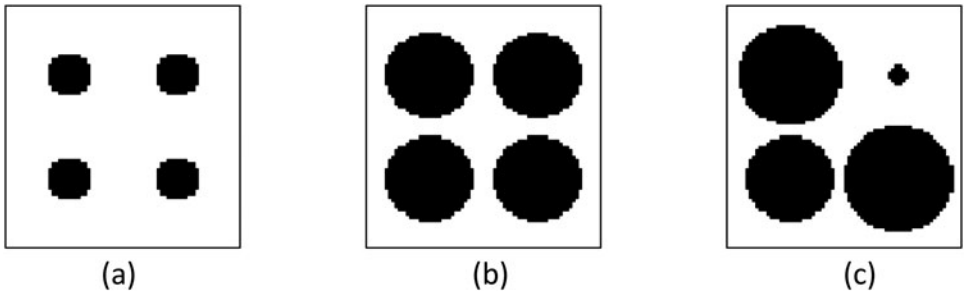

Figure 2. Three simulated images. Window size is normalized to be [0, 1] × [0, 1]. The centers of the agglomerates in all images are {(0.25, 0.25), (0.75, 0.25), (0.25, 0.75), (0.75, 0.75)}. (a) The radius of each agglomerate is 0.1; (b) the radius of each agglomerate is 0.2; (c) the radii of the agglomerates, from top-left to bottom-right, are 0.23, 0.04, 0.2, and 0.25, respectively.

We want to show that if using smaller enough quadrats, the discretization under a discretized version of CSR provides good enough approximation of the K function under the CSR assumption.

Suppose that a TEM image is made up of $S \times S$ pixels. We discretize the image by quadrats of size $k \times k$ pixels, producing $M = (S/k)^2$ number of quadrats in the image. For simplicity, we let S be a multiple of k to avoid using quadrats of a different size near the boundary. Image processing steps already identify the particle agglomerate from the background, so that we can assign a value of 1 for the particle pixels and a value of 0 for all background pixels. We label a quadrat of size $k \times k$ according to the values of majority pixels; if at least $\lfloor \frac{k \times k}{2} \rfloor + 1$ pixels are of value 1, then the quadrat is labeled as a particle quadrat; otherwise, a background quadrat.

Let q denote the fraction of quadrats that are particles. Under the discretized version of CSR, different quadrats are independent from one another, each quadrat has a probability q for being a particle and a probability $1 - q$ for being the background. After the discretization, the centroid coordinates of the particle quadrats are fed into the calculation of the K function.

Let K_{discrete} be the theoretical value of Ripley's K function in the discretized image. Following the definition of the K function, we have

$$K_{\text{discrete}}(r) = \frac{\left(Q\left(\frac{Sr}{k}\right) - 1\right) q}{Mq} = \frac{Q\left(\frac{Sr}{k}\right) - 1}{M}, \tag{7}$$

where $Q(h)$ is the number of quadrats inside the boundary of a circle of radius h.

To show the connection between $K_{\text{discrete}}(r)$ and the original $K(r)$, the key is to understand the function $Q(\cdot)$, which is known as the Gauss circle problem (Hardy 1999), and its solution is given as

$$Q(h) = \pi h^2 + \epsilon(h), \tag{8}$$

where $\|\epsilon(h)\| \le a \cdot h$ and a is a constant.

Recall that under the standard CSR, $K(r) = \pi r^2$. We can show that, under CSR,

$$\begin{aligned} &\|K_{\text{discrete}}(r) - K(r)\| \\ &= \left\| \frac{\pi\left(\frac{S}{k} \cdot r\right)^2 + \epsilon\left(\frac{S}{k} \cdot r\right) - 1}{\left(\frac{S}{k}\right)^2} - \pi r^2 \right\| \\ &= \left\| \frac{\epsilon\left(\frac{S}{k} \cdot r\right) - 1}{\left(\frac{S}{k}\right)^2} \right\| \le \left\| \frac{\epsilon\left(\frac{S}{k} \cdot r\right)}{\left(\frac{S}{k}\right)^2} \right\| + \left(\frac{k}{S}\right)^2 \\ &\le \frac{a \cdot \frac{S}{k} \cdot r}{\left(\frac{S}{k}\right)^2} + \left(\frac{k}{S}\right)^2 = \frac{a \cdot k}{S} r + \left(\frac{k}{S}\right)^2. \end{aligned}$$

For relatively small k's, $K_{\text{discrete}(r)}$ is very close to $K(r)$ under CSR. Figure 3 presents a numerical example in which the image size is normalized to $[0, 1] \times [0, 1]$ and the image is made up of 1024×1024 pixels (i.e., $S = 1024$). We set k to be 512, 128, and 16, respectively, to examine the difference between $K(r)$ and corresponding $K_{\text{discrete}}(r)$. Evidently, $K_{\text{discrete}}(r)$ and $K(r)$ become indistinguishable when k is 16 or smaller.

In practice, 1024×1024 pixels are a typical size of many nano and other material images. For such an image size, the numerical analysis shows that $k = 16$ is sufficiently small. In our later analysis, we choose the value of k based on the physical size of a stand-alone nanoparticle (about 5×5 pixels in size), which is even smaller than a 16×16 quadrat in a 1024×1024-pixel image. For other applications, once given an image size, one can use the above-presented approximation formula to find out how small a k needs to be for discretization and then choose its value accordingly.

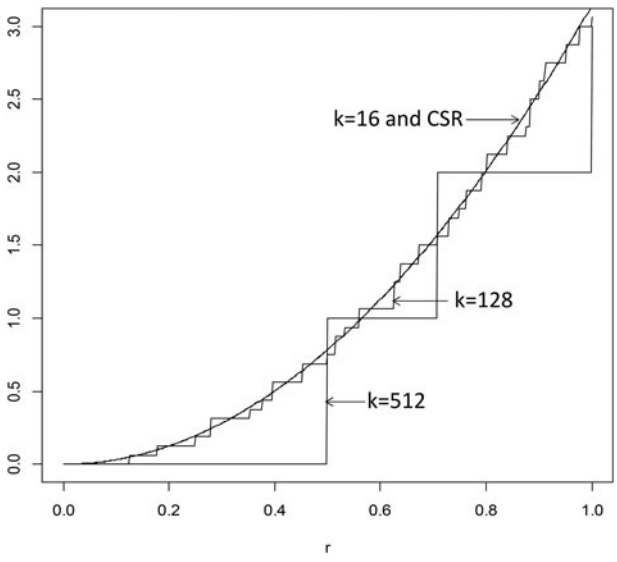

Figure 3. K function under CSR and K_{discrete} with different k's.

3.2 Adjustment of the Normalizing Parameter

The discretization addresses only part of the problems arising from the particle's aggregation. The other part comes from the fact that imaging instruments only measure local areas of a bulk material. When particle aggregates, the intensity of particles observed per local area differs. In the material mixing problem, the nanoparticles blended into the host material are of a known quantity (measured in terms of weight or volume). Under the null hypothesis that the nanoparticles are dispersed and distributed homogenously throughout the host material, the expected number of particles appearing under a given view field of TEM, namely, in a TEM image of the same size, should be the same. When the number of particles in an image is substantially different from that of others, this appearance itself is an indication of inhomogeneity.

When using the K function, including the discretized K function, the normalizing parameter, λ, is the intensity of points per image. If one observes an image containing particles with bad dispersion (large agglomerates) but reasonable distribution (agglomerates spacing evenly), the fact that this local image has more particles (than some other images) does not alert the K function about its implication of inhomogeneity, because the higher local particle intensity will be normalized. On the contrary, the use of a local λ tends to cause the discretized K function to deem an image containing large agglomerates distributed more uniformly, which is quite counter-intuitive.

This can be better understood by looking at the images in Figure 2(a) and (b). When using the original K function, the two images were deemed the same in terms of spatial point distribution, as the size difference of the point agglomerates is simply ignored and their centroid positions are the same. When using the discretized K function, they produce different assessment outcomes, but Figure 2(b), which contains large agglomerates, is considered more uniformly distributed. This is because with the presence of large agglomerates, the denominator of the discretized K function increases, by the amount of extra number of points that the large agglomerates have over the small agglomerates, resulting in a K value closer to CSR. Our numerical analysis confirms this intuition.

So the question becomes what we should use as the normalizing parameter when local images are observed but the global homogeneity is assessed. We believe that a global λ needs to be used. Then, the question is how the global λ can be estimated. We think the estimation is going to be application dependent. In the following, we will discuss how to do this for the material mixing applications, which may be applicable even broadly to other applications. In the cases that the global λ cannot be estimated using the content addition parameters as in the mixing process, we recommend using the average of the local intensities associated with all available view fields (i.e., all local images in an application).

In the material mixing applications, denote by c the volumetric portion of nanoparticles (or other additive agents) that are mixed into a host material. Assume that a nanoparticle occupies a quadrat of size $k \times k$. When nanoparticles are indeed uniformly mixed, the quadrats in the image have probability c to be a particle or probability $1 - c$ to be the background. The closeness measure in the numerator of the K function becomes

$$E\left(\text{number of extra points within distance } r \text{ of a randomly chosen point}\right) = (Q(r) - 1)c. \tag{9}$$

Obviously we need to normalize the above expected value by c, leading to a revised K function, referred to as the $\widetilde{K}$ hereinafter, such that:

$$\widetilde{K} = \frac{E(\text{number of extra points within distance } r \text{ of a randomly chosen point})}{c}. \tag{10}$$

Similar to how the K function is estimated, $\widetilde{K}$ can be estimated as follows:

$$\widehat{\widetilde{K}} = \frac{\frac{1}{N}\sum_{s_1=1}^{N}\sum_{s_2\neq s_1} w_{s_1s_2} I(d_{s_1s_2} < r)}{c}. \tag{11}$$

As such, the global normalizing constant in the material mixing applications is simply the volumetric portion of the additive agents, which can be readily calculated when we know how much host material and additive material are used in the mixing as well as their physical densities.

3.3 Relation Between Discretized K and $\widetilde{K}$

In this subsection, we use a set of simulated images to understand how $\widetilde{K}$ behaves. The image simulation tool that we employ is the Ising model (Winkler 2003), which is developed for characterizing the dependency among spatial binary data based on the theory of Markov random field. Specifically, we use the `PottsUtils` package in R, developed by Feng and Tierney (2014), to generate spatial data samples based on the Ising model and then turn that into a black and white image. One key parameter used in the `PottsUtils` package is called β, which characterizes the aggregating or clustering level of the spatial points. When $\beta = 0$, it means that a given point is independent from its neighboring vertices. The larger the β is, the more clustered the points are. Figure 4 presents a number of image examples simulated using the Ising model with different β's.

We conduct the following analysis using the Ising model-based simulated images:

1. Generate a $B \times B$-pixel image using the Ising model, starting with $\beta = 0$.
2. Estimate c, the global point intensity, using the $B \times B$-pixel whole image, which is to be used in $\widetilde{K}$.
3. Random sample a $b \times b$-pixel subimage from the whole image.
4. Compute the discretized K function for the subimage.
5. Compute the $\widetilde{K}$ function for the subimage using the c estimated in Step 2.
6. Plot the discretized K and $\widetilde{K}$ curves on the same plot.
7. Repeat Steps 3–6 50 times so that discretized K and $\widetilde{K}$ form two clusters of curves.
8. Plot the CSR curve on the same plot.
9. Change β to the next value and repeat Steps 1–8.

In the analysis, we choose $B = 500$ and $b = 50$. The result is presented in Figure 5. Other value combinations were tried but

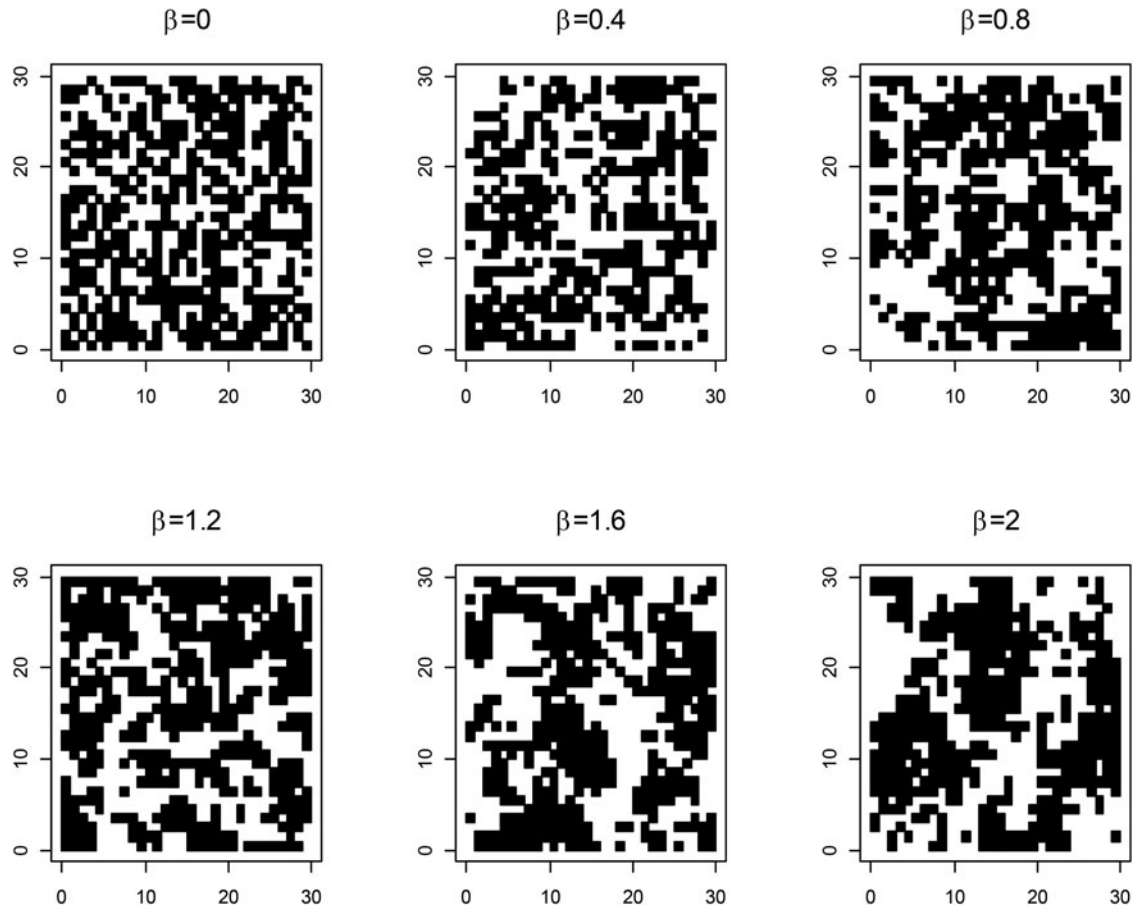

Figure 4. Simulated images using the Ising model with different β values.

the insights are the same, so we omit the plots using other value combinations.

Observing the curves in Figure 5, we notice that when $\beta = 0$, both K curves and $\widetilde{K}$ curves are tightly clustered around the CSR curve, as they should be. When β starts to increase, meaning that the points begin to aggregate, the difference between the two sets of curves becomes more and more pronounced. The $\widetilde{K}$ curves appear sensitive responding to even small nonzero values of β. For the same β, the $\widetilde{K}$ deviates more from the CSR curve and has a greater variability. We anticipate this greater variability in $\widetilde{K}$ curves as $\widetilde{K}$ responds to both dispersion and distribution effects, whereas the discretized K is shrunk by the presence of large point agglomerates.

The third observation is that some (nearly half) of the $\widetilde{K}$ curves lies above the CSR curve, while the others below the CSR curve. By contrast, all discretized K curves are above the CSR curve. It turns out that when the local point density of the subimage is smaller than the global point density c, the resulting $\widetilde{K}$ curve is below the CSR curve, whereas when the local density is larger, the resulting $\widetilde{K}$ is above the CSR curve. This phenomenon of $\widetilde{K}$ is expected, too. In characterizing the mixing homogeneity, one should compare the $\widetilde{K}$ curve to the reference CSR curve: the further it is above the CSR curve or the further it is below the CSR curve both indicate inhomogeneity.

3.4 Nonparametric Test Procedure

When the images of material samples show a difference, practitioners would like to know whether the difference is significant beyond the level of background randomness. The following statistical testing procedure is devised to address this question.

Because we conduct pairwise comparisons in the later analysis, it implies that two groups of images are involved. Let i be the group index and j be the image index within a group. Denote the number of images in the ith group by m_i, so that $i = 1, 2$ and $j = 1, \ldots, m_i$. For each image, a spatial homogeneity characterizing function, including both the original K and the revised $\widetilde{K}$, can be applied. Let N_{ij} denote the number of particles in the jth image of the ith group. Further denote by $N_i = \sum_{j=1}^{m_i} N_{ij}$ the number of particles in the ith group and by $N_t = \sum_{i=1}^{2} N_i$ the total number of particles in the entire comparison.

Diggle, Lange, and Beneš (1991) and Diggle, Mateu, and Clough (2000) proposed two test statistics, D_1 and D_2, to be used, respectively, with Ripley's K function for testing the spatial homogeneity difference between multiple groups of images. We use the same test statistics with K replaced by $\widetilde{K}$. The following expressions follow Diggle, Lange, and Beneš (1991) and Diggle, Mateu, and Clough's (2000) original definition, except that K is replaced by $\widetilde{K}$:

$$D_1 = \sum_{i=1}^{2} \int_0^{r_0} \left(\sqrt{\bar{\widetilde{K}}_i(r)} - \sqrt{\bar{\widetilde{K}}(r)} \right)^2 dr, \tag{12}$$

$$D_2 = \sum_{i=1}^{2} N_i \int_0^{r_0} \frac{1}{r^2} (\bar{\widetilde{K}}_i(r) - \bar{\widetilde{K}}(r))^2 dr, \tag{13}$$

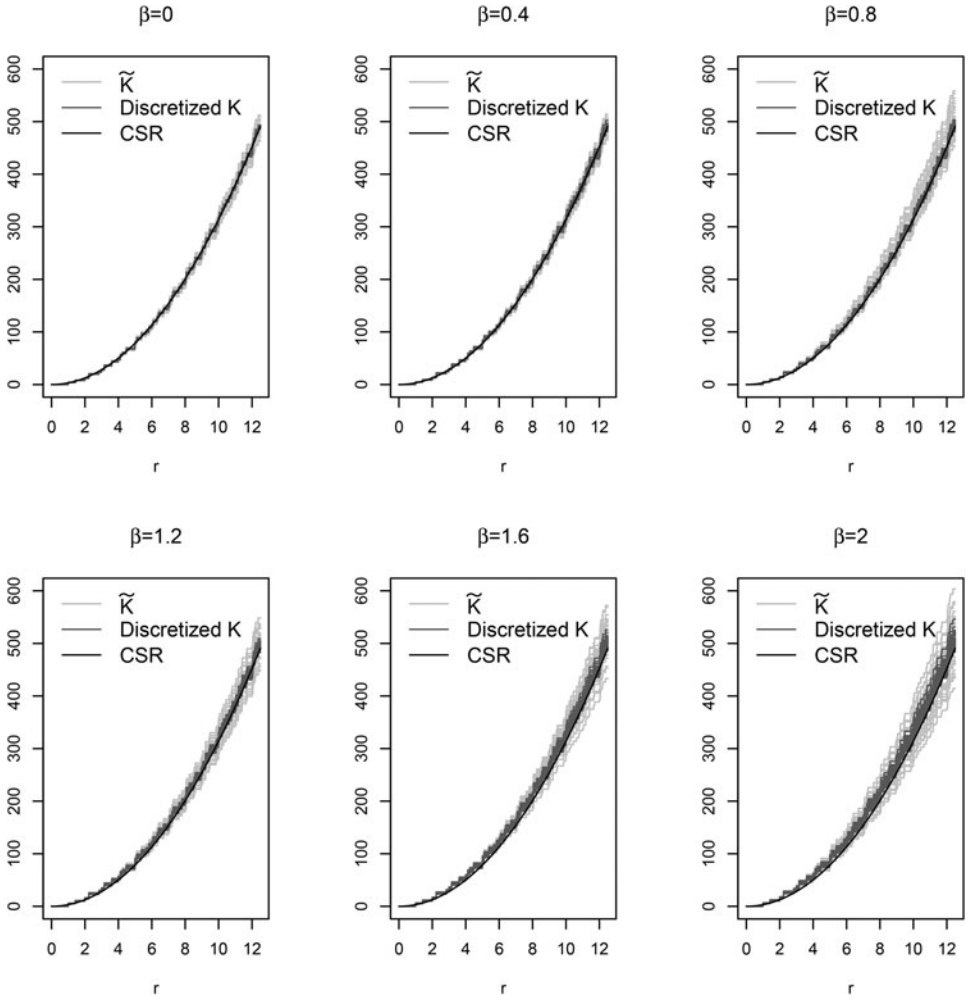

Figure 5. Discretized K versus $\widetilde{K}$ under local image observations and different degrees of point aggregation.

where r_0 is the longest distance with which the $\widetilde{K}$ (or K) is evaluated, and

$$\bar{K}_i(r) = \frac{1}{N_i} \sum_{j=1}^{m_i} N_{ij} \widehat{\widetilde{K}}_{ij}(r), \text{ for } i = 1, 2,$$

and

$$\bar{K}(r) = \frac{1}{N_t} \sum_{i=1}^{2} N_i \bar{K}_i(r) \tag{14}$$

are the average $\widehat{\widetilde{K}}$ within a group and the grand average of the two groups, respectively. The r_0 is often chosen according to Ripley's rule of thumb (Venables and Ripley 2002), where r_0 is one quarter, in size, of the shorter side of the image window. In computation, the above integrals are approximated by the summation of the integrand over one thousand equally spaced r values.

To compute the p-value of the test statistics, Diggle, Lange, and Beneš (1991) initially suggested a bootstrap procedure. But in more recent work (Diggle, Mateu, and Clough 2000), they argued that a permutation procedure works better. In this work, we employ a permutation procedure to compute the statistical significance level of both D_1 and D_2. The permutation test entails the following steps:

1. Apply $\widetilde{K}$ function to each image in the two groups and compute $\widehat{\widetilde{K}}_{ij}$, for $i = 1, 2$ and $j = 1, \ldots, m_i$.
2. Compute D_1 and D_2 statistics using the values from Step 1. Refer to either of the statistics as T_{observed}.
3. Permute the images across the two groups. To do so, we can label the images in the two groups sequentially as $\{1, 2, \ldots, m_1, m_1 + 1, \ldots, m_1 + m_2\}$. Randomly shuffle the sequence of the numbers. Take the images whose labels correspond to the first m_1 numbers in a shuffled set and form the new group 1, while the remaining images form the new group 2.
4. Repeat Steps 1 and 2 on the two new groups. Refer to the resulting statistics as T.
5. Repeat Steps 3 and 4 L times and obtain L values of either statistics, namely T_ℓ, for $\ell = 1, \ldots, L$.
6. Compare T_{observed} with $\{T_\ell\}_{\ell=1}^{L}$. If T_{observed} ranks the eth largest among $\{T_\ell\}_{\ell=1}^{L}$, then the resulting p-value is approximated by $\frac{e}{L}$.

In practice, because of the need to reduce measurement cost and time, there may be sometimes only a single image of the material taken under a given condition. This means that two single images are to be compared with one another to differentiate the spatial homogeneity under their respective conditions. We can in fact still use the steps outlined above to conduct the statistical test by following the image partitioning idea in Hahn

(2012). The action undertaken is to partition each image into 3×3 subimages of equal sizes, so that two groups of images are formed with $m_1 = m_2 = 9$. Then, the statistics and steps presented above can be applied.

A final note is that the nonparametric test statistics for both $\widetilde{K}$ and K are in the form of a sum of squares. In lieu of the observations made in Section 3.3 that $\widetilde{K}$ has a greater variability around the CSR curve as β starts deviating from zero, this implies that $\widetilde{K}$ is more sensitive to signaling point inhomogeneity when inhomogeneity is present.

4. Application to TEM Images

In this section, we conduct a quantification study of the mixing states using TEM images of materials samples. To make the material, butyl acetate, three-functional trimethylolpropane triacrylate and silica nanoparticles are mechanically mixed into silica nanoparticle suspension. Then the suspension is poured to a bead mill machine to further break up nanoparticles; for more details about a typical bead mill process, please refer to Wang and Forssberg (2006). The milling time varies from 5 min to 90 min. After milling, the nanocomposite is diluted by butyl acetate. The reason for dilution is that the nanoparticles in the original material cannot be properly imaged by TEM. Engineers believe that the nanoparticles' mixing state or the clustering level after the dilution is still a good representation of what is in the original material. A drop of the diluted nanoparticle suspension was casted onto a carbon-coated copper grid and dried at room temperature. The mixing and morphology of the nanoparticles were observed using a FEI Tecnai F20 TEM. The nanoparticle content as deposited onto the carbon-coated copper-grid sample holder is 0.00124 in terms of volumetric ratio. The diameter of a stand-alone nanoparticle is around 13 nm.

From the images presented later, it is apparently not true that the longer people run the bead-milling process, the better dispersed and distributed the nanoparticles will be. One question of interest to practitioners is to find out the optimal time length that this bead-milling process needs to run to get the most homogeneous dispersion of nanoparticles. Experiments are conducted with the bead-milling process running for multiple time lengths. TEM images of material samples are taken at each time point.

Two sets of experiments are conducted. In the first one, a single TEM image is taken at six time points of 5, 10, 15, 35, 60, and 90 min, respectively. The TEM image is taken at a randomly chosen location of the material sample. In the second experiment, the same process is executed. This time, engineers want to take images of the material sample at 0 min (i.e., before the bead-milling process runs). Another difference in the second experiment is that multiple images, ranging from 12 to 18 in count, are taken at randomly chosen locations on the sample. To save measurement efforts and costs in the second experiment, two intermediate time points, 15 min and 60 min, are removed. There are no substantial reasons why these two time points are chosen for removal; instead it is done based on the engineer's intuition. We analyze the two circumstances separately.

4.1 A Single Image Taken at a Given Time Point

Figure 6 presents the six single TEM images taken from the material sample at each time point specified above. The images are of 1024×1024 pixels. We use `ImageJ` to extract the centroid locations and area information of each particle or agglomerate. The images are discretized by using $k = 5$; the value of k is chosen so that each quadrat is close to the actual size of a stand-alone nanoparticle (about 13 nanometers in diameter).

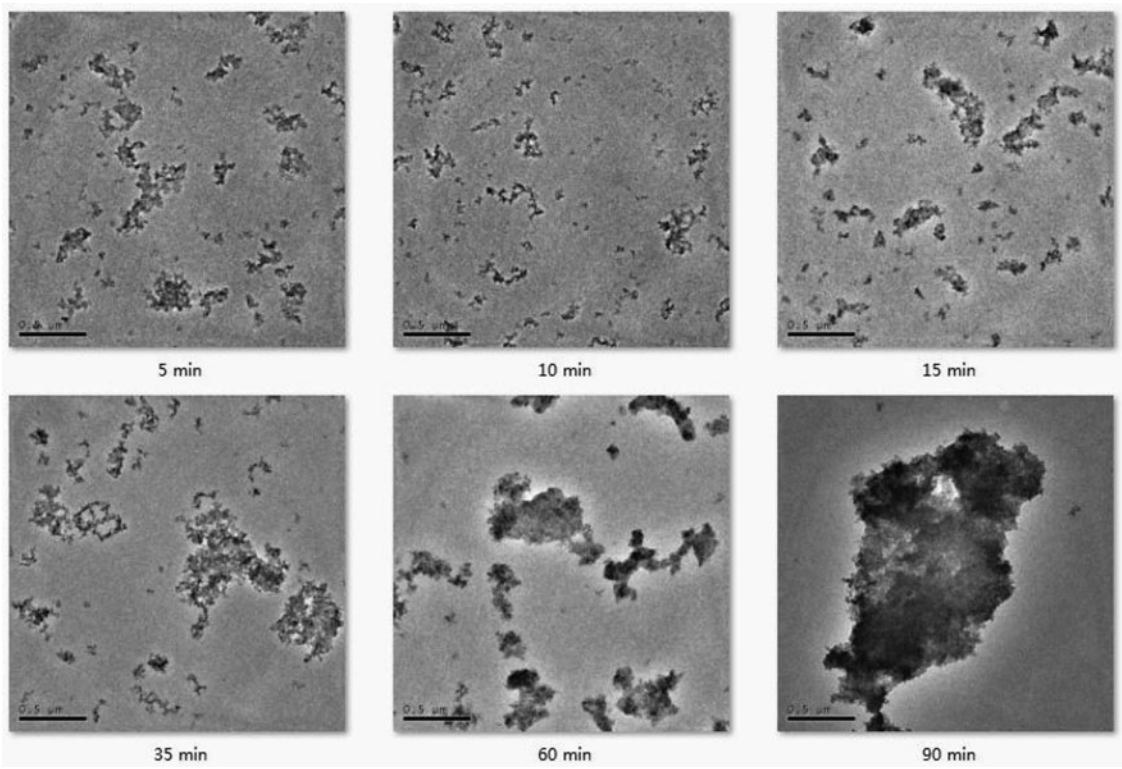

Figure 6. A single TEM image taken of the material sample at each time point.

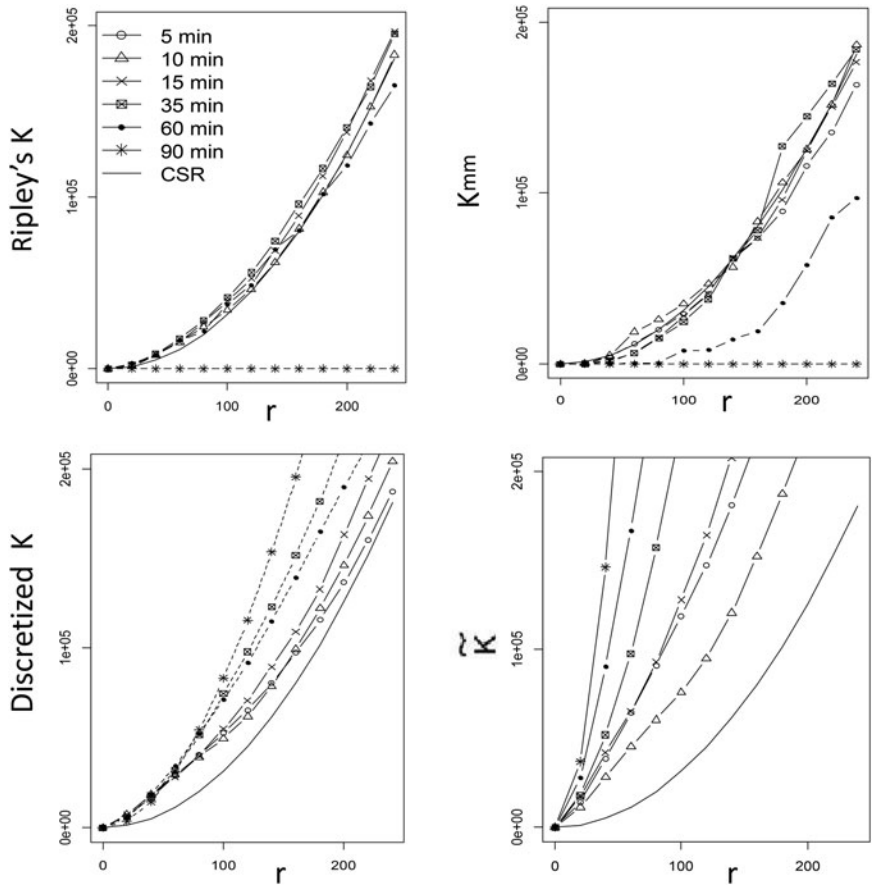

Figure 7. Comparison of Ripley's K function, K_{mm} function, discretized K function, and $\widetilde{K}$ function.

Because 1024 is not divisible by 5, we just discretize a 1020×1020 subimage and set those pixels on the boundary to be the background. The normalizing parameter in $\widetilde{K}$, c, is set to be the actual nanoparticle volumetric ratio, that is, $c = 0.00124$.

For each image, we compute Ripley's K curve, the weighted K_{mm} curve, the discretized K curve, and the $\widetilde{K}$ curve. R package `dbmss` (Marcon et al. 2014) is used to implement the K_{mm} function, while R package `spatstat` is used to compute K. Then, based on K values, we can estimate $\widetilde{K}$ values. For these real images, we use r in the unit of number of image pixels. We set $r_0 = 1024/4 = 256$. Figure 7 presents the seven curves (curves for the six TEM images and the curve under CSR) for each function.

The rank order of spatial homogeneity can be concluded from observing how far a specific curve is away from the curve of the ideal model. When using the original Ripley's K and K_{mm}, most of the curves are clustered on the CSR curve, making it difficult to differentiate the mixing states in the corresponding images. In both Ripley's K and K_{mm} plots, the 90-min curve is a flat line because there is a giant particle agglomerate in the middle with a couple of small particle blocks scattered in the periphery. Because neither Ripley's K nor K_{mm} makes use of the particle agglomerate size information, the agglomerates are simply reduced into dimensionless points at their centroids whose distances in between are greater than r_0. Consequently, their values are always zero for the range of r shown in the plot. K_{mm} curve does differentiate the 60-min state from the rest of the states, as well as from the 90-min state, whereas Ripley's K fails to differentiate anything but the 90-min state.

When the discretization is applied, the discretized K function improves upon both Ripley's K and K_{mm}, as the differences in the curves corresponding to different states are more noticeable. Using the distance away from the CSR curve as the criterion, the discretized K suggests that the order of the mixing state, from most homogenous to least, is 5 min, 10 min, 15 min, 60 min, 35 min, and then, 90 min.

When both discretization and the new normalizing parameter are applied, the $\widetilde{K}$ curves are plotted. The separation of the $\widetilde{K}$ curves is more pronounced, making it easier to tell the difference between two mixing states. The mixing state order suggested by $\widetilde{K}$ appears different from that suggested by discretized K. Using $\widetilde{K}$, one would conclude that the 10 min running of the bead-milling process produces the most homogenous mixing of the particles, followed by 5 min, 15 min, 35 min, 60 min, and then, 90 min.

When presenting these images to a group of material scientists, the 10 min image is unanimously deemed most preferable, while the preference between 5 min and 15 min is evenly split. The preference order over 35 min, 60 min, and 90 min is clearly lower than the other three cases; on this aspect, both $\widetilde{K}$ and discretized K reach the same conclusion. But the difference is that $\widetilde{K}$ favors 35 min over 60 min, whereas discretized K does the opposite. Again, the engineers all agree with the rank order that $\widetilde{K}$ produces.

Table 1. Pairwise comparison using the six TEM images: p-values based on test statistic D_1.

p	5 min	10 min	15 min	35 min	60 min	90 min
5 min	–	0.059	0.695	0.051	<0.001	<0.001
10 min	–	–	0.030	0.003	<0.001	<0.001
15 min	–	–	–	0.057	<0.001	<0.001
35 min	–	–	–	–	0.023	<0.001
60 min	–	–	–	–	–	0.004
90 min	–	–	–	–	–	–

The p-values based on $\widetilde{K}$ for the pairwise comparisons among the six TEM images are presented in Tables 1 and 2. Table 1 includes the results based on D_1, whereas Table 2 is based on D_2. Using either test statistics lead to the same conclusion. The difference between 10 min and 5 min is marginally significant, while the difference between 5 min and 15 min is clearly insignificant. Not surprisingly, the difference between 10 min and 15 min is more significant than that between 10 min and 5 min. The relatively large p-value between 5 min and 15 min provides clues of why engineers could not agree among themselves which case to favor. Other pairs of comparison have reasonably small p-values, indicating significant differences. This suggests that the order between 35 min and 60 min does not happen by chance. In summary, we believe that $\widetilde{K}$ provides the most sensible outcome that is also easy to interpret.

4.2 Multiple Images Taken at a Given Time Point

In the second study, we take several TEM images at randomly chosen locations on a material sample at each given time point. We have 14 images at 0 min, 13 images at 5 min, 12 images at 10 min, 12 images at 35 min, and 18 images at 90 min. Figures 8 shows five images in each row, which are a subset of the images taken at each time point.

We conducted the pairwise comparison analysis, similar to what we have done in the previous subsection. All settings are the same, except that for this study, the test procedure follows that for two groups of images. In the second study, we only use $\widetilde{K}$, as the first study has demonstrated the advantage of $\widetilde{K}$ well over Ripley's K and K_{mm}, and over the discretized K as well.

Figure 9 presents the $\widetilde{K}$ curves resulting from individual images. The $\widetilde{K}$ curves from the two groups are differentiated by using two different line types. To save space, we omit the presentation of pairwise $\widetilde{K}$ curves involving the images at 0 min, as it is obvious that before the bead-milling process is applied, the nanoparticles tend to cluster together heavily. The plots of these pairwise $\widetilde{K}$ curves shed lights in terms of how significantly two groups of images are different from each other. Based on the plots, it is apparent that the images of 5 min is noticeably different from the other three groups. The other groups are generally not that much different, while some of them may be marginally different (e.g., 10 min versus 90 min).

Table 2. Pairwise comparison using the six TEM images: p-values based on test statistic D_2.

p	5 min	10 min	15 min	35 min	60 min	90 min
5 min	–	0.049	0.582	0.038	<0.001	<0.001
10 min	–	–	0.018	0.002	<0.001	<0.001
15 min	–	–	–	0.049	<0.001	<0.001
35 min	–	–	–	–	0.015	<0.001
60 min	–	–	–	–	–	0.004
90 min	–	–	–	–	–	–

Table 3. Pairwise comparison using the five groups of TEM images: p-value based on D_1.

p	0 min	5 min	10 min	35 min	90 min
0 min	–	0.004	0.066	0.401	0.838
5 min	–	–	0.050	0.003	0.006
10 min	–	–	–	0.213	0.154
35 min	–	–	–	–	0.633
90 min	–	–	–	–	–

Tables 3 and 4 present the p-values when pairwise comparison is made between two groups of images. In these two tables, the images at 0 min are included in the comparison. Images at 0 min are shown to be indeed different from those at 5 min and 10 min but not so much different from those at 35 min and 90 min. For the images taken at 5 min, 10 min, 35 min, and 90 min, the implications resulting from D_1 and D_2 are consistent with each other and they are also consistent with the plots in Figure 9. Generally speaking, images taken at 5 min show a better mixing state of nanoparticles than any other images (including those at 0 min). Images taken at 10 min, 35 min, and 90 min are not that different, while images of 10 min could be marginally different from that of 90 min.

Altogether, this analysis suggests that the bead-milling process does make a difference to the mixing state of nanoparticles. Consistent with the general trend shown in the first experiment, the second experiment also shows that the nanoparticles start to disperse, once the bead-milling operation runs, but will recluster if the operation runs beyond certain time.

The difference, though, is that the best mixing state in the second experiment is chosen at 5 min of the bead-milling operation, while that in the first experiment is chosen at 10 min. A closer look at the images taken in the two experiments suggests that the conclusion in the second experiment, based on a group of images, is likely to be more robust. The particle mixing states have a great variability over the material sample. Conclusion based on a single image could be misleading. To see this, consider comparing the right most image in Figure 8, row (b), with the right most image in Figure 8, row (c). Then, consider comparing the right most image in Figure 8, row (b), with the middle image in Figure 8, row (c). These two comparisons would yield opposite conclusions. With more than 12 images per group in the second experiment, such bias, albeit unlikely disappearing altogether, should have been alleviated as compared to the circumstance of a single image per time point used in the first experiment.

Table 4. Pairwise comparison using the five groups of TEM images: p-value based on D_2.

p	0 min	5 min	10 min	35 min	90 min
0 min	–	0.002	0.027	0.337	0.790
5 min	–	–	0.038	<0.001	<0.001
10 min	–	–	–	0.165	0.071
35 min	–	–	–	–	0.520
90 min	–	–	–	–	–

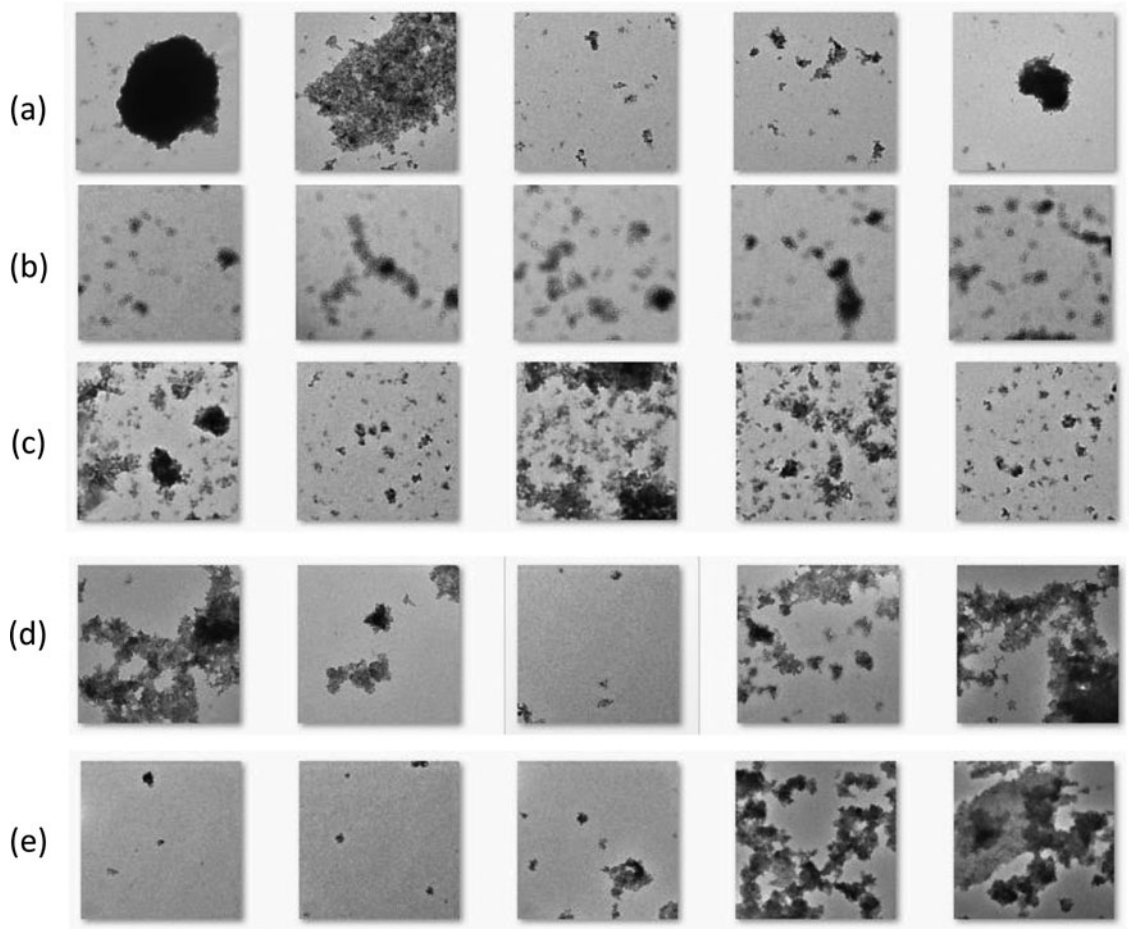

Figure 8. (a) through (e) are subsets of images taken at 0 min, 5 min, 10 min, 35 min, and 90 min, respectively.

As mentioned just above, the bead-milling process does break down the agglomerates into smaller pieces of nanoparticle aggregates and disperse them over the material sample. One unexpected phenomenon is that when the bead-milling operation lasts too long, it could create new agglomerates of a large size. Based on the two experiments, it seems unlikely that one needs to run the bead-milling operation for longer than 35 min, as the optimal mixing states take place at an early stage. The optimum is difficult to be pinpointed yet but it most probably happens between 5 and 10 min of the operation. Because of this, the removal of image-taking at 15 min in the second experiment may not matter a lot. Still, in retrospective, it would have been a safer approach, had the engineer removed the image-taking at 35 min but kept that at 15 min.

5. Summary

We propose a revised spatial homogeneity characterizing function for quantification purpose in material mixing applications. This revised function is based on Ripley's K function but incorporates two major revisions: (1) the function is applied to a material sample image after discretization and (2) the normalizing parameter in the characterizing function is the global point intensity estimated for the bulk material. When applying the revised function to two case studies using real TEM images taken from material samples, the revised function differentiates the mixing states consistently with engineering intuition and engineers' preference, while the original K function fails to do so. The use of the revised characterizing function helps identify a proper time range for an important nanomanufacturing operation to produce desirable outcome in terms of nanoparticles mixing quality.

One point we made earlier is about the robustness of conclusions when having multiple images versus having a single image at a given time point. It comes as no surprise that using multiple images is more desirable. On the other hand, people recognize the extra time and cost associated with the measurement procedure when multiple images are taken and used. Naturally it raises a number of sample-taking related questions, such as how many images are needed to safeguard the quality of the conclusion and what the best sequence may be to take multiple images at a given time point. For instance, is the random sampling the best approach to use? Solution to these questions appears not straightforward and is outside the scope of this article. We plan to treat them in our ongoing pursuit.

A final note is concerning the limitation of the conclusions made based on 2D images. One potential problem may come from the sample preparation process. When a drying process is used while preparing material samples for TEM images, that process could possibly change the amount of clusters or produce additional agglomerates. When a 3D solid sample is used, the 2D projection of the possibly multiple layers of nanoparticles in the 3D sample may produce artifacts of particle agglomerates, too.

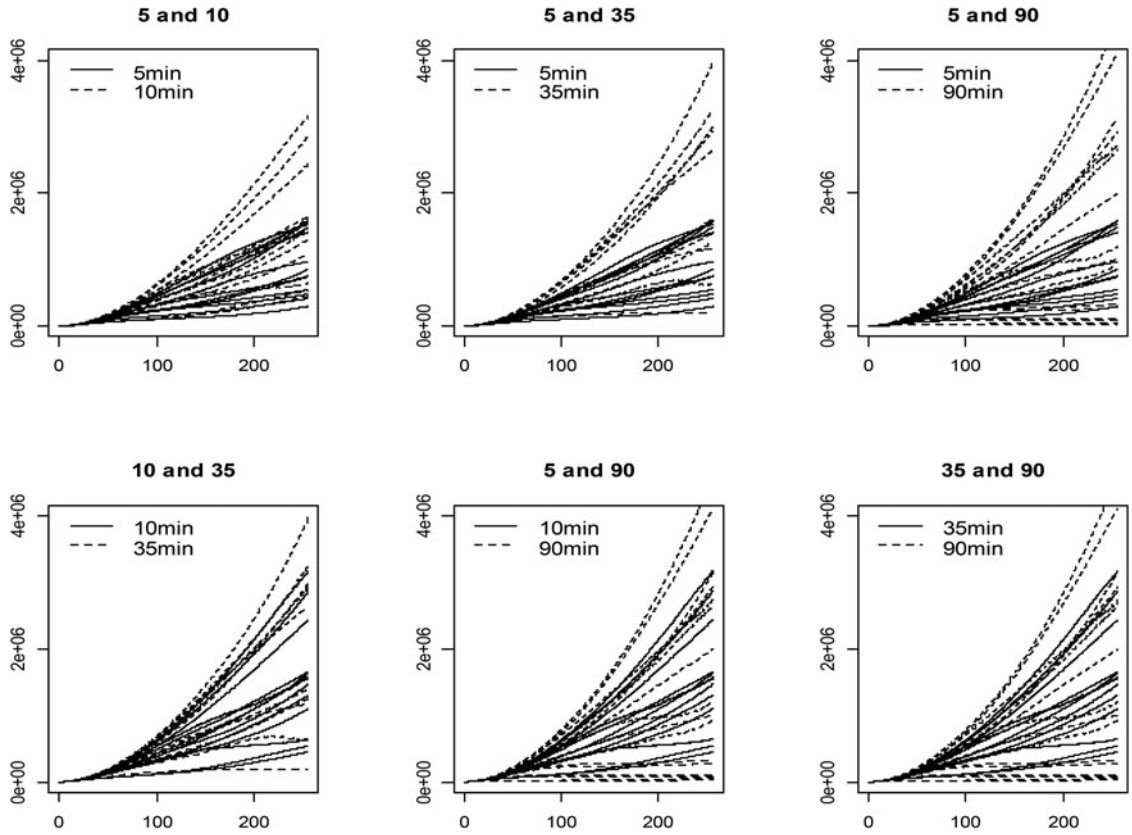

Figure 9. Pairwise $\widetilde{K}$ curves using images taken at 5 min, 10 min, 35 min, and 90 min. Horizontal and vertical axes represent r values and the correscponding $\widetilde{K}(r)$ values, respectively.

There is also a general need to make a 2D-to-3D inference, for which we note that some initial efforts have been made by Zhou et al. (2014) and Li et al. (2014).

Acknowledgments

The authors acknowledge the generous support from their sponsors. Qian and Ding are partially supported by NSF under grant no. CMMI-1000088. The authors are grateful to Professor Xiaoying Qi and Mr. Pengfei Chu of the National Center for Nanoscience and Technology, Beijing, China, for providing the image data used in the article.

References

Baddeley, A. (2008), "Analysing Spatial Point Patterns in R," Technical Report, The Commonwealth Scientific and Industrial Research Organisation(CSIRO). Available at *http://www.csiro.au/resources/pf16h*. [392]

Baddeley, A., Møller, J., and Waagepetersen, R. (2000), "Non- and Semi-Parametric Estimation of Interaction in Inhomogeneous Point Patterns," *Statistica Neerlandica*, 54, 329–350. [392]

Chang, L., Zhang, Z., Zhang, H., and Schlarb, A. K. (2006), "On the Sliding Wear of Nanoparticle Filled Polyamide 66 Composites," *Composites Science and Technology*, 66, 3188–3198. [391]

Diggle, P. J., and Chetwynd, A. G. (1991), "Second-Order Analysis of Spatial Clustering for Inhomogeneous Populations," *Biometrics*, 47, 1155–1163. [392]

Diggle, P. J., Lange, N., and Beneš, F. M. (1991), "Analysis of Variance for Replicated Spatial Point Patterns in Clinical Neuroanatomy," *Journal of the American Statistical Association*, 86, 618–625. [392,396,397]

Diggle, P. J., Mateu, J., and Clough, H. E. (2000), "A Comparison Between Parametric and Non-Parametric Approaches to the Analysis of Replicated Spatial Point Patterns," *Advances in Applied Probability*, 32, 331–343. [392,396,397]

Diggle, P. J., Tawn, J. A., and Moyeed, R. A. (1998), "Model-Based Geostatistics," *Journal of the Royal Statistical Society*, Series C, 47, 299–350. [392]

Feng, D., and Tierney, L. (2014), "PottsUtils: Utility Functions of the Potts Models," *R Package Version 0.3-2*. Available at *http://CRAN.R-project.org/package=PottsUtils*. [395]

Ferreira, T., and Rasband, W. (2011), *The ImageJ User Guide*, Bethesda, MD: National Institutes of Health. Available at *http://rsb.info.nih.gov/ij/*. [391]

Hahn, U. (2012), "A Studentized Permutation Test for the Comparison of Spatial Point Patterns," *Journal of the American Statistical Association*, 107, 754–764. [398]

Hardy, G. H. (1999), *Ramanujan: Twelve Lectures on Subjects Suggested by His Life and Work* (3rd ed.), New York: Chelsea. [394]

Hui, L., Smith, R., Wang, X., Nelson, J., and Schadler, L. (2008), "Quantification of Particulate Mixing in Nanocomposites," in *Annual Report Conference on Electrical Insulation and Dielectric Phenomena (CEIDP)*, IEEE, pp. 317–320. [391]

Li, X., Zhang, H., Jin, J., Huang, D., Qi, X., Zhang, Z., and Yu, D. (2014), "Quantifying Dispersion of Nanoparticles in Polymer Nanocomposites Through Transmission Electron Microscopy Micrographs," *Journal of Micro and Nano-Manufacturing*, 2, 021008. [392,402]

Lotwick, H. W., and Silverman, B. W. (1982), "Methods for Analysing Spatial Processes of Several Types of Points," *Journal of the Royal Statistical Society*, Series B, 406–413. [392]

Manas-Zloczower, I. (1997), "Analysis of Mixing in Polymer Processing Equipment," *Rheology Bulletin*, 66, available at *http://www.rheology.org/sor/publications/rheology_b/jan97/mixing.pdf*. [391,393]

Marcon, E., Lang, G., Traissac, S., and Puech, F. (2014), "Dbmss: Distance-Based Measures of Spatial Structures," *R Package Version 2.1.2*. Available at *http://CRAN.R-project.org/package=dbmss*. [399]

Park, C., Huang, J. Z., Huitink, D., Kundu, S., Mallick, B. K., Liang, H., and Ding, Y. (2012), "A Multistage, Semi-Automated Procedure for Analyzing the Morphology of Nanoparticles," *IIE Transactions*, 44, 507–522. [391]

Park, C., Huang, J. Z., Ji, J. X., and Ding, Y. (2013), "Segmentation, Inference and Classification of Partially Overlapping Nanoparticles," *IEEE Transactions on Pattern Analysis and Machine Intelligence*, 35, 669–681. [391]

Penttinen, A., Stoyan, D., and Henttonen, H. M. (1992), "Marked Point Processes in Forest Statistics," *Forest Science*, 38, 806–824. [392,393]

Ray, S. S., and Okamoto, M. (2003), "Polymer/Layered Silicate Nanocomposites: A Review From Preparation to Processing," *Progress in Polymer Science*, 28, 1539–1641. [391]

Ripley, B. D. (1976), "The Second-Order Analysis of Stationary Point Processes," *Journal of Applied Probability*, 255–266. [391]

——— (1991), *Statistical Inference for Spatial Processes*, New York: Cambridge University Press. [393]

Stoyan, D., and Penttinen, A. (2000), "Recent Applications of Point Process Methods in Forestry Statistics," *Statistical Science*, 15, 61–78. [392]

Venables, W. N., and Ripley, B. D. (2002), *Modern Applied Statistics With S*, New York: Springer Science & Business Media. [397]

Wang, Y., and Forssberg, E. (2006), "Production of Carbonate and Silica Nanoparticles in Stirred Bead Milling," *International Journal of Mineral Processing*, 81, 1–14. [398]

Winkler, G. (2003), *Image Analysis, Random Fields and Dynamic Monte Carlo Methods: A Mathematical Introduction* (2nd ed.), New York: Springer. [395]

Zeng, Q., Yu, A., and Lu, G. (2008), "Multiscale Modeling and Simulation of Polymer Nanocomposites," *Progress in Polymer Science*, 33, 191–269. [391]

Zhang, H., Zhang, Z., Friedrich, K., and Eger, C. (2006), "Property Improvements of in Situ Epoxy Nanocomposites With Reduced Interparticle Distance at High Nanosilica Content," *Acta Materialia*, 54, 1833–1842. [391]

Zhou, Q., Zhou, J., De Cicco, M., Zhou, S., and Li, X. (2014), "Detecting 3D Spatial Clustering of Particles in Nanocomposites Based on Cross-Sectional Images," *Technometrics*, 56, 212–224. [392,402]

Zou, H., Wu, S., and Shen, J. (2008), "Polymer/Silica Nanocomposites: Preparation, Characterization, Properties, and Applications," *Chemical Reviews*, 108, 3893–3957. [391]